The *in-silico* evaluation of important GLUT9 residue for uric acid transport based on renal hypouricemia type 2

Raul Cachau[1], **Shahin Shahsavari**[2], **Sung Kweon Cho**[3,4]

[1]Integrated Data Science Section, Research Technologies Branch, National Institute of Allergies and Infectious Diseases, Bethesda, MD, USA.

[2]Geisel School of Medicine at Dartmouth, Hanover, NH, USA

[3]Center for Cancer Research, National Cancer Institute, Frederick, MD, USA.

[4]Department of Pharmacology Ajou University, School of Medicine, Suwon, Korea.

Abstract

Uric acid is the end product of purine metabolism. Uric acid transporters in the renal proximal tubule plays a key role in uric acid transport. Functional abnormalities in these transporters could lead to high or low levels of uric acid in the blood plasma, known as hyperuricemia and hypouricemia, respectively. *GLUT9* has been reported as a key transporter for uric acid reuptake in renal proximal tubule. *GLUT9* mutation is known as causal gene for renal hypouricemia due to defective uric acid uptake, with more severe cases resulting in urolithiasis and exercise induced acute kidney injury (EIAKI). However, the effect of mutation is not fully investigated and hard to predict the change of binding affinity. We comprehensively described the effect of *GLUT9* mutation for uric acid transport using molecular dynamics and investigated the specific site for uric acid binding diffeferences. R171C and R380W showed the significant disruption of the

Corresponding author Sung Kweon Cho, MD, PhD, Department of Pharmacology, Ajou University School of Medicine, 164, Worldcup-ro, Yeongtong-gu, Suwon, 16499, South Korea, Tel: +82-31-219-4506; Fax: +82-31-219-5069; wontan2000@gmail.com.
Authorship contributions
Category 1
Conception and design of study: Raul Cachau, Sung Kweon Cho;
Acquisition of data: Raul Cachau, Shahin Shahsavari, Sung Kweon Cho;
analysis and/or interpretation of data: Raul Cachau, Sung Kweon Cho;
Category 2
Drafting the manuscript: Raul Cachau, Sung Kweon Cho;
revising the manuscript critically for important intellectual content: Raul Cachau, Sung Kweon Cho;
Category 3
Approval of the version of the manuscript to be published (the names of all authors must be listed): Raul Cachau, Shahin Shahsavari, Sung Kweon Cho

AUTHORSHIP STATEMENT
All persons who meet authorship criteria are listed as authors, and all authors certify that they have participated sufficiently in the work to take public responsibility for the content, including participation in the concept, design, analysis, writing, or revision of the manuscript. Furthermore, each author certifies that this material or similar material has not been and will not be submitted to or published in any other publication before its appearance in the Hong Kong Journal of Occupational Therapy.
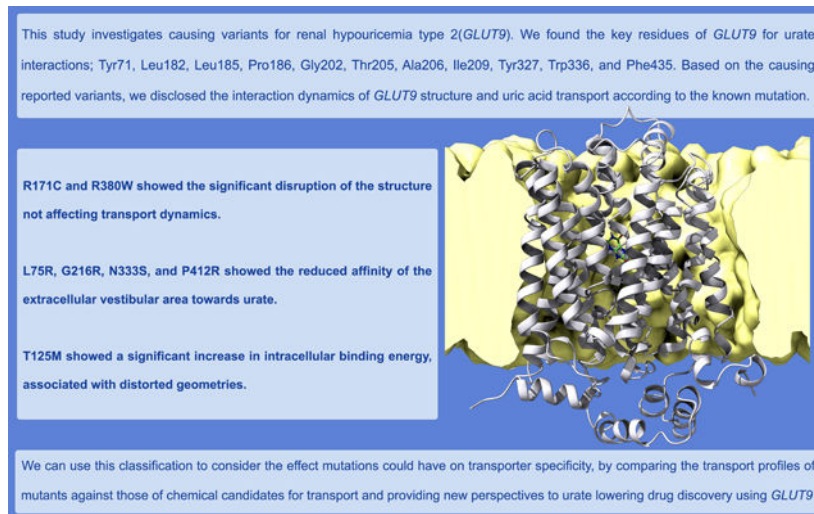
Declaration of interests
The authors declare the following financial interests/personal relationships which may be considered as potential competing interests:

structure not affecting transport dynamics whereas L75R, G216R, N333S, and P412R showed the reduced affinity of the extracellular vestibular area towards urate. Interestingly, T125M showed a significant increase in intracellular binding energy, associated with distorted geometries. We can use this classification to consider the effect mutations by comparing the transport profiles of mutants against those of chemical candidates for transport and providing new perspectives to urate lowering drug discovery using GLUT9

Graphical Abstract

This study investigates causing variants for renal hypouricemia type 2(*GLUT9*). We found the key residues of *GLUT9* for urate interactions; Tyr71, Leu182, Leu185, Pro186, Gly202, Thr205, Ala206, Ile209, Tyr327, Trp336, and Phe435. Based on the causing reported variants, we disclosed the interaction dynamics of *GLUT9* structure and uric acid transport according to the known mutation.

R171C and R380W showed the significant disruption of the structure not affecting transport dynamics.

L75R, G216R, N333S, and P412R showed the reduced affinity of the extracellular vestibular area towards urate.

T125M showed a significant increase in intracellular binding energy, associated with distorted geometries.

We can use this classification to consider the effect mutations could have on transporter specificity, by comparing the transport profiles of mutants against those of chemical candidates for transport and providing new perspectives to urate lowering drug discovery using *GLUT9*

Keywords

GLUT9; Hypouricemia; Molecular dynamics

1 Introduction

Renal hypouricemia type 2 (RHUC2, OMIM: 612076) is an inherited disorder characterized by impaired renal urate reabsorption and hypouricemia due to impairment of the glucose transporter 9 (GLUT9). People with RHUC2 have increased risk of developing urolithiasis and/or exercise-induced acute renal failure (EIARF). Typically, RHUC2 is diagnosed as serum uric acid less than 2 mg/dl and fractional excretion uric acid (FeUA) higher than 10%[1]. Different *GLUT9* variants have been reported in different populations, including East Asian, Roma, Israeli-Arab, and Ashkenazi Jewish[2–7]. The mode of *GLUT9* variant inheritance is known as autosomal recessive. Two isoforms are reported, known as *GLUT9a* and *GLUT9b. GLUT9a* encodes 540 amino acids with 12 exons, and *GLUT9b* encodes 511 amino acids with 13 exons. The two variant sequences differ in the N-terminus: *GLUT9a* contains an N-terminal dileucine motif. *GLUT9a* is localized in the liver and basolateral side of the renal proximal tubule, whereas *GLUT9b* is localized on the apical side in the collecting duct and placenta. Uric acid transport through *GLUT9a* and *GLUT9b* has the same kinetics (K_m for uric acid ~0.6 mM), and is not affected by the glucose and fructose substrates. Genome-wide association studies (GWAS) have shown that *GLUT9*, *URAT1*, *OAT4*, *ABCG2, and OAT10* are associated with serum uric acid (SUA), FE-UA, gout, and

body mass index, and *GLUT9* genetic variants are responsible for a portion of the variance in SUA concentrations (5–6% in females and 1–2% in males)[8,9]. Identification of key residues in *URAT1* that interacted with uric acid led to the development of urate-lowering therapeutics. We reviewed the clinical evidence linking RHUC2 with its related *GLUT9* variants. We use this information to predict the effects of specific amino acid changes on the *GLUT9* structure, and present the binding affinities of each residue for uric acid, chloride, ascorbate and glucose to assess the impact of localized changes in the transport properties of *GLUT9*.

2 Methods

2.1 In silico analysis of novel missense variants

Known pathogenic variants of *GLUT9* were screened in the Human Gene Mutation Database (HGMD). We performed evolutionary conservation analysis of missense *GLUT9* variants across vertebrate orthologs using the UCSC Genome Browser (https://genome.ucsc.edu/). Nitrogen excretion has a functional role in the evolutionary process, and we identified mutated amino acid sequences in several mammals (*Rhesus macaque*, *Mus musculus*, and *Canis lupus familiaris*). Finally, we predicted the functional effects of missense variants using the Annotation, Visualization, and Impact Analysis webserver (AVIA v3.0, https://avia.abcc.ncifcrf.gov)[10]. Minor allele frequency information was collected from The Genome Aggregation Database (gnomAD v2.1.1)[11]. Several methods were used for the prediction of mutants properties including DUET, PolyPhen-2 (Polymorphism Phenotyping v2), SIFT (Sorting Intolerant from Tolerant), Condel (Consensus Deleteriousness Score of Nonsynonymous Single Nucleotide Variants), and Mutation Taster[12–16]. The result of these explorations were inconclusive with some surprising trends revealed. For instance, we found SIFT to be highly tolerant of proline mutations[17].

2.2 *GLUT9* Strutural modeling

GLUT9 belongs to a subset of solute carrier family of transporters with a Rocker Switch (RS) alternating-access transport mechanism. To date, there is no experimental structure of *GLUT9* available. However, several experimental structures of other RS GLUT transporters are available, including outward-open (GLUT1, PDB ID: 5EQG; GLUT3, PDB ID: 4ZWC; GLUT5, PDB ID:4YBQ), inward-open (GLUT3, PDB ID: 4ZW9; GLUT5, PDB ID: 4YB9), and complexes including sugars and other compounds (GLUT3-maltose, PDB ID: 4ZWC; GLUT1-cytochalasin, PDB ID: 5EQI; GLUT1-nonyl beta-D-glucopyranoside, PDB ID:4PYP).

We built models to simulate *GLUT9* transport properties. The initial *GLUT9* models were generated with the YASARA (Yet Another Scientific Artificial Reality Application) package[18] using homology modeling macro (HM_build) based on 25 templates, 10 alternative sequence alignments, and 50 loops per model. Taken together, 372 of 457 (81.4%) of the long-form target residues were aligned to template residues. The sequence identity among aligned residues was 43.3%, and the sequence similarity (measured by BLOSUM62 score > 0) was 62.4%. A target sequence profile was created with PSI-BLAST

(Position-Specific Iterative Basic Local Alignment Search Tool) and then analyzed with the PSI-Pred secondary structure prediction algorithm[19]. Since the prediction for the N-terminal segment of long-form *GLUT9* did not provide sufficient information to build a model, we made the hybrid model using YASARA HM_build macro obtained from all modeling engines (I-TASSER[20], Rosetta[21], Phyre2[22], Swiss-Model[23], YASARA[18] and AlphaFold2 -without the use of templates). The hybrid model was further refined against all templates using FRMD (Feedback Restrain Molecular Dynamics)[24,25], which improved the *Z*-scores for the outward-open and inward-open forms from –0.67 to –0.65 and –0.7 to –0.68, respectively. The overall arrangement of the *GLUT9* WT is shown at Fig. 1.

2.3 Molecular dynamics and assessment of *GLUT9* mutations

Simulations were performed in membranes made of 20% cholesterol and 80% phospholipids (33% phosphatidylethanolamine; 33% phosphatidylcholine and 14% phosphatidylserine)[26]. Stabilization trajectories were conducted for 50 ns, followed by 250 ns production runs using the YASARA MD_run macro in the semi-isotropic NPT default ensemble (temperature of 298K and a pressure of 1 atm). Model flexibility and stability were assessed using the YASARA MD_analyze macro. Steered dynamics (Yasara md_runsteered) was used extensively to explore the properties of the models. The equations of motions for all steered dynamics simulations were integrated with a multiple timestep of 1.25 fs for bonded intractions and 2.5 fs for non-bonded interactions at NPT ensemble.

After an equilibration time of 3 ps, a minimum acceleration of 2000 pm/ps^2 was applied to all steered atoms together with the non-bonded forces (every 2.5 fs). Considering the steered mass (M) in Dalton this results in a pulling force of [2000*M*0.00166] picoNewton. The pulling direction was defined by a vector manually provided to point right out of the binding pocket (i.e. for the driving of substrate), and continuously updated to account for rotations of the complex. The maximum distance between the centers of mass of receptor and ligand was continuously updated upto 400 simulation steps. The acceleration was increased by 500 pm/ps^2. As soon as the maximum distance grew faster than MaxDisSpeed =4000 m/s (i.e. a barrier was overcome and nothing prevented the ligand from accelerating), the acceleration was scaled down by a factor of $1-(1-4000/\text{MaxDisSpeed})^2$, but not below the initial minimum. This check was done every 20 simulation steps. The simulation was stopped when the ligand had moved 15 Å away or the model has morphed into its final geometry. Large displacemetns (i.e. invertion barrier) were treated in a similar fashion with the displacement vectors updated automatically. RMSD-biased steering was also considered. Relative binding energies were computed over the production trajectories using the md_analyzebindenergy macro and solvation-corrected with Molecular mechanics Poisson–Boltzmann surface area (MM-PBSA)[27]. Steered dynamics were used to guide GLUT9 WT trajectories (12 replicas in each direction) through the inward/outward inversion process (Fig. 2) computed in the outward to inward geometry inversion process.

DUET[16] and mCMS were used to assess the impact of mutations on structural stability, but the results were unexpectedly insensitive to the mutation considered. Molecular dynamics calculations were used to evaluate the model stability and transport of mutants. These

calculations were YASARA v20.4.24[18] with the Amber14 force field, including the Lipid14 set and standard parameters used in the md_membrane macro.

2.4 The simulation of urate and anion transport in *GLUT9*

The modeling of rigid substrates transport is challenging because rigid substrates (i.e., urate) cannot easily reorient (tumble) as they are confined along the transport path. The spontaneous flipping of these substrates requires a long time for the reorientation to occur. Furthermore, molecular dynamics simulations of urate diffusion to the mouth of the transporter region does not suggest a preferable orientation at the initial steps of the transport process. To address this problem, we approached the simulation of transport properties using steered dynamics using 12 replicas to expedite sampling to the transport path, starting from four nonequivalent substrate orientations (up/down, left flipping/right flipping) in the case of dehydroascorbate (DHA) and urate, while considering each tautomeric form separately. Two tautomeric forms were considered for DHA and four tautomeric forms were considered for urate, as predicted by the Tautomerizer web service[28] (Fig. 3). We also explored the contribution of polarization to the urate binding and transport profile by performing MOPAC16/PM7 calculations[29]. These calculations included the first layer of water molecules bound to the protein and the COSMO reaction field model, and followed the recommended protocol including an initial constrained relaxation of the model as described by Brandon et al.[30]. A suitable reference for binding energy calculations was created by placing the substrate in a sphere containing 512 water molecules, subsequently optimized by molecular dynamics, and then subjected to the same treatment as applied to the protein-substrate complex using MOPAC/PM7/COSMO. MOPAC calculations were used to estimate binding energies for the extreme points (energy maxima and minima) observed during the steered dynamics. The polarization energy contribution was measured as the difference between the molecular mechanics and the MOPAC estimated binding energies, and accounted for up to 20% and 7% or less of the total binding energies for urate and DHA, respectively. We also tested the *GLUT9* substrates (glucose and urate) and negative controls (Chrolin and DHA) for the comparison.

3 Results

3.1. Clinical reports for *GLUT9* variants of RHUC2

A list of *GLUT9* amino acid changes associated with RHUC2 is presented in Table 1. The *GLUT9* variants were reported in multiple ethnic groups. Most were reported as case studies of renal hypouricemia, except for two missense variants (p.V282I and p.R294H). These two were common variants identified by A Genome-Wide Association Study (GWAS). These variants lowered uric acid levels to prevent gout, and were not associated with RHUC2[31].

The p.L75R mutation was reported in an Israeli-Arab case that presented as nephrolithiasis and exercise-induced acute renal failure (EIARF). The p.T125M and p.R171C mutations were discovered during a routine blood test in an Israeli-Arab case that did not show any clinical presentations. The p.R198C and p.P412R mutations were discovered in a Japanese case. The p.R380W mutation was discovered in Korean and Japanese cases who presented

with EIARF and nephrolithiasis[32]. The p.G216R and p.N333S mutations were reported in a Roma case who presented with EIARF.

3.2. In-silico prediction of *GLUT9* mutation properties

The functional effects of the *GLUT9* mutation were predicted using Mutation Taster, CLINVAR, Polyphen-2, and CADD v1.6. The two common variants (p.V282I and p.R294H) were predicted to be benign, whereas the rare variants (p.L75R, p.T125M, p.R171C, p.R198C, p.G216R, p.G236*, p.N333S, p.R380W, and p.P412R) were pathogenic, disease-causing or damaging. The CADD score predictions of variants are reported in Table 1. We further evaluated the effects of the amino acid changes using molecular modeling.

3.3. *GLUT9* modeling result

The variety of available structures favor the use of homology modeling methods to model RS *GLUT* transporters. RS *GLUT* transporters had a characteristic pseudo C2 symmetry arrangement with internal subsymmetries relating to the 12 transmembrane-spanning helices (Fig. 1 bottom). This arrangement aligned helices 2/11 and 5/8 via the C2 symmetry in a parallel configuration. The two pseudosymmetric arrangements were connected between helices 6 and 7 on the cytoplasmatic side. The arrangement displayed subsymmetries within each separate domain that could facilitate domain swapping–mediated oligomerization. We also explored *GLUT9* association in the membrane, which was performed by in-silico coarse-grain modeling[10] to simulate the in-membrane dimerization process, with similar results. Nevertheless, the simulations suggested the most probable association may occur between helices 5/6 and 9/12 resulting from a lateral translation. The interaction energy estimate for this interaction was <5 kcal/mol, which may not be sufficient to stabilize large aggregates. No evident functional impact on the *GLUT9* transport properties can be drawn from these association models.

Sequence similarities among RS *GLUT* transporters are recognizable, although a comparative analysis of the *GLUT1* to *GLUT4* series indicated that each member displays a characteristic binding profile[11]. We speculated that these differences extended to RS *GLUT* mutant transport profiles, although the modulation of transport preferences by single point mutations had not been systematically explored. Cheng[33] successfully applied modeling tools to the transport of species other than sugars (e.g., urate, dehydroascorbate). *GLUT9* structure was modeled using a simple scheme by Clemencon[34], and docking experiments on static homology models were performed[35]; however, no *GLUT9* transport modeling studies have been reported. This energy contribution may be significant but does not result in different selectivity profiles; although, it may provide a more accurate measurement of the transport process energetics. All WT and mutant *GLUT9* models displayed narrower vestibular areas than the *GLUT1* and *GLUT3* experimental structures (PDB ID: 5EQG; PDB ID: 4ZW9). We challenged this arrangement using RMSD-biased steered dynamics and the experimental *GLUT1* structures as templates to guide the structural geometry toward arrangements with larger vestibular volumes. These chimeric arrangements returned to their initial structures in less than 250 ns of the molecular dynamics simulation, suggesting that the observed narrower arrangements may be characteristic of *GLUT9*. The inversion energy barrier obtained for the glucose-bound GLUT9 WT was estimated as >15 kcal/mol unless

the solvent dynamics in the vestibular areas were included in the steering protocol. A 3 kcal/mol barrier was obtained when both the solvent and overall shape were used to drive structural reorganization in the steering protocol. A limited number of simulations applied the same protocol to the apo form, and the results suggested a much higher inversion barrier (>20 kcal/mol) in the absence of a bound substrate, which was probably exaggerated due to the difficult migration of the water molecules. Nevertheles, this exploratory work suggests an active role for the bound substrate in facilitating *GLUT9* inversion, which is in agreement with previous reports[36,37].

The final binding energies are summarized in Table 2. This describes the substrate migration from the bulk solvent to the vestibular area outer region, a barrier to the internal binding site (described by the highest energy point obtained during the transit of the substrate to its binding site), and the lowest energy found in the internal binding site. This approach simplifies the description of the substrate binding process and was used to describe both the inward-facing and outward-facing geometries. These estimates were dependent on the state of protonation of the internal Tyr71 and Tyr327 residues, which we consider protonated as independently predicted by PROPKA[38] and YASARA pKa prediction calculations. Based on known regidue for hypouricemia, we constructed the *GLUT9* structrual model for uric acid transport (Fig 4.).

3.4. The prediction of *GLUT9* mutant effect

It is important to point out some of the limitations of the models presented for a proper assessment of the results. Some mutations, like R380W, may result in partial unfolding, affecting protein transport and membrane insertion. The modeling strategy presented will have a general tendency to over stabilize these models and experimental verification of protein stability will be performed in the future. Similarly, the models presented do not provide sufficient sampling to asses the effect of membrane lipid segregation and its possible effect in the transporter properties. We are extending the modeling studies to obtain longer molecular dynamics trajectories to address some of these questions. The narrow scope of the panel presented in Table 1 is to gather general information that could guide our understanding of the possible modulation of the transporter properties by single point mutations, including how these changes may affect its specificity overall. We further analyzed these mutations based on their impact on *GLUT9* transport properties by modeling the appropriate mutant (Table 2) and relating them to their placement in the binding region and whether they altered the substrate-binding, or whether they modified the transport mechanism by perturbing the dynamics or overall arrangement of the transporter. For example, mutations that perturbed the selectivity filter/binding site (i.e., L75R and N333S) or impacted the vestibular areas (i.e., R198C) may alter the transporter specificity but not affect transporter dynamics. Binding energy changes suggested that all these mutations had a negative effect on binding energies for glucose (1–3 kcal/mol) and urate (3–6 kcal/mol), with glucose seemingly less affected by these mutations. Alternatively, mutants affecting *GLUT9* structure, but not directly involved in binding of the transported substrate, may change the overall properties by affecting the transporter structure or modifying the transporter dynamics. For example, the T125M mutation had a large effect on the structural dynamics and indirectly affected the transport properties (Table 2). Mutations that affected

the overall structure can impact the transporter selectivity to different molecules. The Ile335 mutation selectively lowered fructose transport[39] even though the residue was buried in a hydrophobic pocket that stabilized the helical bundle. The effect can be explained by the resulting perturbation of the substrate-binding region due to the dislocation of the structurally stable helical bundle as shown in our modeling of this residue mutation to alanine, resulting in a <ΔRMSD> value of 5.3A where <ΔRMSD> was computed by comparing the values obtained in the WT vs. mutant in a molecular dynamics trajectory, which is a measure of the disorder introduced into the structure by the mutation). Mutations that affected the vestibular areas altered the electrostatic properties, such as R171C, and had a seemingly similar effect as the R380W mutation as measured by <ΔRMSD>. However, the mechanism by which transport was affected differed in each case. The R171C mutation modified the properties of the outward-facing vestibular area by changing the overall dynamics of the region, and molecular dynamics simulations of the R380W mutant model suggested that this mutation affected transport by breaking a well-structured chain of 12 charged resides involving Lys, Arg, Tyr, and Glu (no Asp are involved) spanning more than 20 A and stabilizing the intracellular domain. This very polar structure had a crucial role in directing anions to the intracellular vestibular area. The R380W mutation affected the inward-facing binding site and decreased the binding energy of urate to −1.2 kcal/mol. The dislodging of this domain also impacted the inversion barrier (Table 2).

3.5. Urate, DHA, and glucose binding sites

Table 3 demonstrated the binding affinity by mutant and the substrate. The binding region was defined by the mean residence time of the substrate during molecular dynamics calculations and the occurrence of long-lived interactions (i.e., hydrogen bonds) with the residue side chains, followed by visual exploration. Our results indicated that the binding sites for urate, DHA, and glucose varied significantly. Clemencon[34] and Salgado Ferreira[35] differed in their descriptions of the glucose binding site: the former was based on a comparative analysis with published structures, whereas the latter analyzed a rigid docking of the substrate. Both analyses identified Tyr327, Phe435, and Trp459 as contributing to substrate binding and the stability of the inner structure of *GLUT9*. Asn333 primarily involved in forming hydrogen bonds with all three substrates. We identified other residues involved in glucose binding using molecular dynamics sampling of the interactions (Fig. 5, Top), including Tyr71, Leu75, Ile209, Cys210, Val213, Leu332, Trp336, Glu364, Phe426, and Asn458. Our analysis differs from previous interpretations of a two-state model with well-differentiated and static exofacial and endofacial binding sites, suggesting a more extended region of *GLUT9* contributed to the binding and recognition of glucose, extending Ainsley[17] interpretation of GLUT transport occurring as a series of binding events.

Urate binding involved contact with many residues (Fig. 5 Bottom), including the previously identified Tyr327, Phe435, and Trp336, and engaged residues Tyr71, Leu182, Leu185, Pro186, Gly202, Thr205, Ala206, Ile209, and Gly432. Tyr71, Ile209, Tyr327, and Trp336 were involved in both glucose and urate interactions. Many residues in the *GLUT9* lumen were involved in the substrate recognition process, which may explain why the transporter can accommodate various substrates and achieve broad specificity profiles. However, the ability to transport organic anions did not appear to be linked to the accumulation of

residues with positive charges, which explains the inability of *GLUT9* to transport chlorine anions. DHA transport can be seen as combining urate and glucose sites with the DHA ring occupying some of the space filled by urate, and the DHA hydrophilic chain extended toward the sugar-binding region.

3.6. Possible transport specificity changes due to mutations

Broad specificity profiles have been characterized for many glucose transporters as successfully applied modeling tools to the transport of species other than sugars (e.g., urate, dehydroascorbate) by *GLUT* transporters, demonstrating the ability of modeling approaches to analyze differences in their transport mechanism[40,41]. The broad specificity of these transporters may result in a possible change of the transport profile upon mutation. We organized our results in order to address this question. We can cluster our results in terms of the effect of the mutation in the extracellular binding of the molecular moiety transported; the impact in the inversion barrier controlling the rocking inversion process, or the binding and release of the chemical from the intracellular vestibular area. R171C and R380W, for instance, show the most significant disruption of the canonical structure as measured by $< \Delta RMSD>$, altering the ability of the transporter to invert. L75R, G216R, N333S, and P412R, on the other hand, modify the affinity of the extracellular vestibular area towards urate, as seen in the increased internal barrier in the outward facing vestibular area. T125M, on the other hand, shows a significant increase in intracellular binding energy, suggesting a more favorable transit of the intracellular vestibular area. However, it should be noted that T125M has a large $<\Delta RMSD>$, suggesting these energies are associated with distorted geometries. It is interesting to notice that T125M does not belong to the same category as R171C and R380W, as seen by the very different impact of the mutation on the inversion barrier.

We can use this classification to consider the effect mutations could have on transporter specificity, by comparing the transport profiles of mutants against those of chemical candidates for transport. Table 2 (bottom) reports the simulated transport characteristics for the wild type against several chemicals, including urate, glucose, dehydro-ascorbate, and chlorine. The transport of glucose shows remarkablely differet from urate. This shows that vestibular regions of *GLUT9* is more favorable to the binding of urate. In addition, the chemical motif's total charge seems to impact the binding energy, as seen when DHA is also considered and emphasized by the binding energies obtained for chlorine anion. The lowering of the vestibular internal barriers, on the other hand, seems to correlate with the ability of the transported motif to form hydrogen bonds, as emphasized again by the inability of chlorine anion to transit between local minima in an effective manner. This transport can be further exemplified by P412R, which results in an urate transport profile in the outward facing vestibular area closer to that of glucose in the wild type. Mutations resulting in larger disruptions of the structure, such as T125M, R171C and R380W, seem to increase the binding affinity for glucose and DHA which may facilitate their transport. Further studies are necessary to fully exploit these differences in the way mutations effectively alter *GLUT9* transport properties. Yet, another consequence of the observed properties of the modeled structures is the possibility of rescuing structure altering mutants (those with larger $<\Delta RMSD>$) using designed chemicals that may restore the overall stability of the transporter, using binding sites away from the vestibular areas. Mutations directly

affecting the binding of urate or glucose offer a more challenging scenario to restore the transporter function via chemical interventions. The differences in the profiles observed for urate, glucose, dehydro-ascorbate (Table 2, bottom), in combination with the changes in the transport profile obtained for the different mutants considered, strongly suggest mutations can change the transporter specificity profile, adding complexity to the emerging phenotype while opening new forms of diagnosis by analyzing transport profiles.

4.   Discussion

GLUT9 encodes a member of the glucose transporter family (also known as *SLC2A9*) that has an essential role in the transport of uric acid in the liver and the kidney [42,43]. *GLUT9* has two isoforms with different localizations[44]. Unlike GLUT transporters, *GLUT9* is a uniport transporter of uric acid in a negative charge form (urate)[45]. Uricosuric agents such as benzbromarone and probenecid inhibit uric acid transport in a voltage-dependent manner[46,47]. Our study showed that *GLUT9* was a rocker switch alternating-access transporter with a well-defined pseudo C2 symmetry topology. The rocking mechanism depended on the presence of a bound substrate, in agreement with previous studies of other rocking transporters[36,37]. *GLUT9* vestibular regions were smaller than those in *GLUT1* and *GLUT3* structures, with more accessible binding pockets.

The mechanism of *GLUT9* binding of glucose and fructose has been debated in previous reports[48,49]. We identified specific residues (Ile335 and Trp110) involved in fructose transport, which may be associated with nonalcoholic fatty liver disease (NAFLD)[50]. Nonsense, frameshift, and canonical ±1 or ±2 splice site mutations are generally assumed to disrupt gene function compared to missense mutations[32]. The extended region showed a large degree of constrained plasticity, which allowed *GLUT9* adaptation to various substrates. We speculated that mutations in this region may alter transport selectivity and enable transport of new substrates as predicted by our models. However, these transport profile changes have not been systematically characterized in GLUT transporters. We are currently exploring experimental approaches to assess transport profile modulation by mutants including the use of chemical libraries to identify compounds with characteristic transport properties.

The extended binding region and the seemingly small effects of several mutants in the overall transporter structure and dynamics indicates that some of these mutants perturb urate transport and potentially modulate transporter selectivity. A new paradigm for the harmful effects of some of these mutations revealed new intervention target through the discovery of occluded pathologies. Conversely, these results support the possibility of changing the transporter efficacy by modulating substrate binding/transport through new strategies to rescue mutants that affect transporter structure/dynamics expanding the possibilities for therapeutic interventions.

In summary, we described the molecular changes involved in compound heterozygous mutations of *GLUT9* leading to hypouricemia. Our clinical and molecular results may expand our understanding of the physiology of renal uric acid transport. We also propose candidate genes for hypouricemia based on unexplained cases.

Supplementary Material

Refer to Web version on PubMed Central for supplementary material.

Acknowledgements

Abbreviation

ABCG2	ATP-Binding Cassette transporter G2
BLOSUM	BLOcks SUbstitution Matrix
Condel	Consensus Deleteriousness Score of Nonsynonymous Single Nucleotide Variants
COSMO	COnductor-like Screening MOdel
DHA	Dehydroascorbic acid
EIARF	Exercise-Induced Acute Renal Failure
FeUA	Fractional Excretion Uric Acid
FRMD	Feedback Restrain Molecular Dynamics
GLUT9	GLUcose Transporter 9
GWAS	A Genome-Wide Association Study
HGMD	Human Gene Mutation Database
MM-PBSA	Molecular Mechanics Poisson–Boltzmann Surface Area
MOPAC	Molecular Orbital PACkage
NAFLD	Non-Alcoholic Fatty Liver Disease
OAT4	Organic Anion Transporter 4
OAT10	Organic Anion Transporter 10
PolyPhen-2	Polymorphism Phenotyping v2
PSI-BLAST	Position-Specific Iterative Basic Local Alignment Search Tool
RHUC2	Renal HypoUriCemia type 2
RMSD	Root-Mean-Square Meviation
RS	Rocker Switch
SIFT	Sorting Intolerant from Tolerant

URAT1	URAte Transporter 1
YASARA	Yet Another Scientific Artificial Reality Application

References

1. Ichida K, Hosoyamada M, Hisatome I, et al. Clinical and molecular analysis of patients with renal hypouricemia in Japan-influence of URAT1 gene on urinary urate excretion. Journal of the American Society of Nephrology. 2004;15(1):164–173. [PubMed: 14694169]

2. Sebesta I, Stiburkova B, Bartl J, et al. Diagnostic tests for primary renal hypouricemia. Nucleosides, nucleotides & nucleic acids. 2011;30(12):1112–1116.

3. Stiburkova B, Taylor J, Marinaki AM, Sebesta I. Acute kidney injury in two children caused by renal hypouricaemia type 2. Pediatric Nephrology. 2012;27(8):1411–1415. [PubMed: 22527535]

4. Dinour D, Bahn A, Ganon L, et al. URAT1 mutations cause renal hypouricemia type 1 in Iraqi Jews. Nephrology, Dialysis, Transplantation. 2011;26(7):2175–2181.

5. Tasic V, Hynes AM, Kitamura K, et al. . Clinical and functional characterization of URAT1 variants. PLoS One. 2011;6(12):e28641-e28641.

6. Stiburkova B, Sebesta I, Ichida K, et al. Novel allelic variants and evidence for a prevalent mutation in URAT1 causing renal hypouricemia: biochemical, genetics and functional analysis. European Journal of Human Genetics : EJHG. 2013;21(10):1067–1073. [PubMed: 23386035]

7. Bhasin B, Stiburkova B, De Castro-Pretelt M, Beck N, Bodurtha JN, Atta MG. Hereditary renal hypouricemia: a new role for allopurinol? The American journal of medicine. 2014;127(1):e3–e4.

8. Cha DH, Gee HY, Cachau R, et al. Contribution of SLC22A12 on hypouricemia and its clinical significance for screening purposes. Sci Rep. Oct 7 2019;9(1):14360. doi:10.1038/s41598-019-50798-6

9. Cho SK, Kim B, Myung W, et al. Polygenic analysis of the effect of common and low-frequency genetic variants on serum uric acid levels in Korean individuals. Sci Rep. Jun 8 2020;10(1):9179. doi:10.1038/s41598-020-66064-z

10. Vuong H, Che A, Ravichandran S, Luke BT, Collins JR, Mudunuri US. AVIA v2.0: annotation, visualization and impact analysis of genomic variants and genes. Bioinformatics. Aug 15 2015;31(16):2748–50. doi:10.1093/bioinformatics/btv200

11. Karczewski KJ, Francioli LC, Tiao G, et al. The mutational constraint spectrum quantified from variation in 141,456 humans. Nature. May 2020;581(7809):434–443. doi:10.1038/s41586-020-2308-7

12. Adzhubei IA, Schmidt S, Peshkin L, et al. A method and server for predicting damaging missense mutations. Nat Methods. Apr 2010;7(4):248–9. doi:10.1038/nmeth0410-248 [PubMed: 20354512]

13. Kumar P, Henikoff S, Ng PC. Predicting the effects of coding non-synonymous variants on protein function using the SIFT algorithm. Nat Protoc. 2009;4(7):1073–81. doi:10.1038/nprot.2009.86 [PubMed: 19561590]

14. Gonzalez-Perez A, Lopez-Bigas N. Improving the assessment of the outcome of nonsynonymous SNVs with a consensus deleteriousness score, Condel. Am J Hum Genet. Apr 08 2011;88(4):440–9. doi:10.1016/j.ajhg.2011.03.004 [PubMed: 21457909]

15. Schwarz JM, Cooper DN, Schuelke M, Seelow D. MutationTaster2: mutation prediction for the deep-sequencing age. Nat Methods. Apr 2014;11(4):361–2. doi:10.1038/nmeth.2890 [PubMed: 24681721]

16. Pires DE, Ascher DB, Blundell TL. DUET: a server for predicting effects of mutations on protein stability using an integrated computational approach. Nucleic Acids Res. Jul 2014;42(Web Server issue):W314–9. doi:10.1093/nar/gku411

17. Ng PC, Henikoff S. SIFT: Predicting amino acid changes that affect protein function. Nucleic Acids Res. Jul 1 2003;31(13):3812–4. doi:10.1093/nar/gkg509 [PubMed: 12824425]

18. Krieger E, Vriend G. YASARA View - molecular graphics for all devices - from smartphones to workstations. Bioinformatics. Oct 15 2014;30(20):2981–2. doi:10.1093/bioinformatics/btu426

19. Jones DT. Protein secondary structure prediction based on position-specific scoring matrices. J Mol Biol. Sep 17 1999;292(2):195–202. doi:10.1006/jmbi.1999.3091 [PubMed: 10493868]

20. Yang J, Zhang Y. I-TASSER server: new development for protein structure and function predictions. Nucleic Acids Res. Jul 1 2015;43(W1):W174–81. doi:10.1093/nar/gkv342 [PubMed: 25883148]

21. Das R, Baker D. Macromolecular modeling with rosetta. Annu Rev Biochem. 2008 2008;77:363–82. doi:10.1146/annurev.biochem.77.062906.171838 [PubMed: 18410248]

22. Kelley LA, Mezulis S, Yates CM, Wass MN, Sternberg MJ. The Phyre2 web portal for protein modeling, prediction and analysis. Nat Protoc. Jun 2015;10(6):845–58. doi:10.1038/nprot.2015.053

23. Waterhouse A, Bertoni M, Bienert S, et al. . SWISS-MODEL: homology modelling of protein structures and complexes. Nucleic Acids Res. Jul 2 2018;46(W1):W296–W303. doi:10.1093/nar/gky427 [PubMed: 29788355]

24. Cachau RE, Gussio R, Beutler JA, et al. Solution Structure of Taxol Determined Using a Novel Feedback-Scaling Procedure for Noe-Restrained Molecular-Dynamics. International Journal of Supercomputer Applications and High Performance Computing. Spr 1994;8(1):24–34. doi:Doi 10.1177/109434209400800104

25. Yokoyama S, Cai Y, Murata M, et al. A novel pathway of LPS uptake through syndecan-1 leading to pyroptotic cell death. Elife. Dec 7 2018;7e37854. doi:10.7554/eLife.37854

26. Boesze-Battaglia K, Schimmel R. Cell membrane lipid composition and distribution: implications for cell function and lessons learned from photoreceptors and platelets. J Exp Biol. Dec 1997;200(Pt 23):2927–36. doi:10.1242/jeb.200.23.2927

27. Genheden S, Ryde U. The MM/PBSA and MM/GBSA methods to estimate ligand-binding affinities. Expert Opin Drug Discov. May 2015;10(5):449–61. doi:10.1517/17460441.2015.1032936 [PubMed: 25835573]

28. Dhaked DK, Ihlenfeldt WD, Patel H, Delannee V, Nicklaus MC. Toward a Comprehensive Treatment of Tautomerism in Chemoinformatics Including in InChI V2. J Chem Inf Model. Mar 23 2020;60(3):1253–1275. doi:10.1021/acs.jcim.9b01080 [PubMed: 32043883]

29. Stewart JJ. Optimization of parameters for semiempirical methods VI: more modifications to the NDDO approximations and re-optimization of parameters. J Mol Model. Jan 2013;19(1):1–32. doi:10.1007/s00894-012-1667-x [PubMed: 23187683]

30. Brandon CJ, Martin BP, McGee KJ, Stewart JJP, Braun-Sand SB. An approach to creating a more realistic working model from a protein data bank entry. Journal of Molecular Modeling. Jan 2015;21(1)3. doi:10.1007/s00894-014-2520-1 [PubMed: 25620422]

31. Pavelcova K, Bohata J, Pavlikova M, Bubenikova E, Pavelka K, Stiburkova B. Evaluation of the Influence of Genetic Variants of SLC2A9 (GLUT9) and SLC22A12 (URAT1) on the Development of Hyperuricemia and Gout. J Clin Med. Aug 4 2020;9(8)doi:10.3390/jcm9082510

32. Yoon J, Cachau R, David VA, et al. Characterization of a Compound Heterozygous SLC2A9 Mutation That Causes Hypouricemia. Biomedicines. Sep 6 2021;9(9)doi:10.3390/biomedicines9091172

33. Cheng KJ, Selvam B, Chen LQ, Shukla D. Distinct Substrate Transport Mechanism Identified in Homologous Sugar Transporters. J Phys Chem B. Oct 10 2019;123(40):8411–8418. doi:10.1021/acs.jpcb.9b08257 [PubMed: 31498631]

34. Clémençon B, Lüscher BP, Fine M, et al. Expression, purification, and structural insights for the human uric acid transporter, GLUT9, using the Xenopus laevis oocytes system. PLoS One. 2014;9(10):e108852. doi:10.1371/journal.pone.0108852 [PubMed: 25286413]

35. Ferreira RS, Pons JL, Labesse G. Insights into Substrate and Inhibitor Selectivity among Human GLUT Transporters through Comparative Modeling and Molecular Docking. ACS Omega. Mar 31 2019;4(3):4748–4760. doi:10.1021/acsomega.8b03447 [PubMed: 32462103]

36. Fu X, Zhang G, Liu R, et al. Mechanistic Study of Human Glucose Transport Mediated by GLUT1. J Chem Inf Model. Mar 28 2016;56(3):517–26. doi:10.1021/acs.jcim.5b00597 [PubMed: 26821218]

37. Latorraca NR, Fastman NM, Venkatakrishnan AJ, Frommer WB, Dror RO, Feng L. Mechanism of Substrate Translocation in an Alternating Access Transporter. Cell. Mar 23 2017;169(1):96–107 e12. doi:10.1016/j.cell.2017.03.010 [PubMed: 28340354]

38. Olsson MH, Sondergaard CR, Rostkowski M, Jensen JH. PROPKA3: Consistent Treatment of Internal and Surface Residues in Empirical pKa Predictions. J Chem Theory Comput. Feb 8 2011;7(2):525–37. doi:10.1021/ct100578z [PubMed: 26596171]

39. Long W, Panwar P, Witkowska K, et al. . Critical Roles of Two Hydrophobic Residues within Human Glucose Transporter 9 (hSLC2A9) in Substrate Selectivity and Urate Transport. J Biol Chem. Jun 12 2015;290(24):15292–303. doi:10.1074/jbc.M114.611178 [PubMed: 25922070]

40. Jumper J, Evans R, Pritzel A, et al. Highly accurate protein structure prediction with AlphaFold. Nature. 2021/08/01 2021;596(7873):583–589. doi:10.1038/s41586-021-03819-2 [PubMed: 34265844]

41. Han L, Qu Q, Aydin D, et al. Structure and mechanism of the SGLT family of glucose transporters. Nature. 2022/01/01 2022;601(7892):274–279. doi:10.1038/s41586-021-04211-w [PubMed: 34880492]

42. Caulfield MJ, Munroe PB, O'Neill D, et al. SLC2A9 is a high-capacity urate transporter in humans. PLoS Med. Oct 7 2008;5(10):e197. doi:10.1371/journal.pmed.0050197 [PubMed: 18842065]

43. Anzai N, Ichida K, Jutabha P, et al. Plasma urate level is directly regulated by a voltage-driven urate efflux transporter URATv1 (SLC2A9) in humans. J Biol Chem. Oct 3 2008;283(40):26834–8. doi:10.1074/jbc.C800156200 [PubMed: 18701466]

44. Vitart V, Rudan I, Hayward C, et al. SLC2A9 is a newly identified urate transporter influencing serum urate concentration, urate excretion and gout. Nat Genet. Apr 2008;40(4):437–42. doi:10.1038/ng.106

45. Barrett MP, Walmsley AR, Gould GW. Structure and function of facilitative sugar transporters. Curr Opin Cell Biol. Aug 1999;11(4):496–502. doi:10.1016/s0955-0674(99)80072-6 [PubMed: 10449337]

46. Bibert S, Hess SK, Firsov D, et al. Mouse GLUT9: evidences for a urate uniporter. Am J Physiol Renal Physiol. Sep 2009;297(3):F612–9. doi:10.1152/ajprenal.00139.2009 [PubMed: 19587147]

47. Enomoto A, Kimura H, Chairoungdua A, et al. Molecular identification of a renal urate anion exchanger that regulates blood urate levels. Nature. May 23 2002;417(6887):447–52. doi:10.1038/nature742

48. Augustin R, Carayannopoulos MO, Dowd LO, Phay JE, Moley JF, Moley KH. Identification and characterization of human glucose transporter-like protein-9 (GLUT9): alternative splicing alters trafficking. J Biol Chem. Apr 16 2004;279(16):16229–36. doi:10.1074/jbc.M312226200 [PubMed: 14739288]

49. Manolescu AR, Augustin R, Moley K, Cheeseman C. A highly conserved hydrophobic motif in the exofacial vestibule of fructose transporting SLC2A proteins acts as a critical determinant of their substrate selectivity. Mol Membr Biol. Sep-Dec 2007;24(5-6):455–63. doi:10.1080/09687680701298143 [PubMed: 17710649]

50. DeBosch BJ, Kluth O, Fujiwara H, Schürmann A, Moley K. Early-onset metabolic syndrome in mice lacking the intestinal uric acid transporter SLC2A9. Nat Commun. Aug 7 2014;5:4642. doi:10.1038/ncomms5642 [PubMed: 25100214]

Highlights

This study investigates causing variants for renal hypouricemia type 2(*GLUT9*). We found the key residues of *GLUT9* for urate interactions; Tyr71, Leu182, Leu185, Pro186, Gly202, Thr205, Ala206, Ile209, Tyr327, Trp336, and Phe435. Based on the causing reported variants, we disclosed the interaction dynamics of *GLUT9* structure and uric acid transport according to the known mutation.

1. R171C and R380W showed the significant disruption of the structure not affecting transport dynamics.

2. L75R, G216R, N333S, and P412R showed the reduced affinity of the extracellular vestibular area towards urate.

3. T125M showed a significant increase in intracellular binding energy, associated with distorted geometries.

We can use this classification to consider the effect mutations could have on transporter specificity, by comparing the transport profiles of mutants against those of chemical candidates for transport and providing new perspectives to urate lowering drug discovery using *GLUT9*
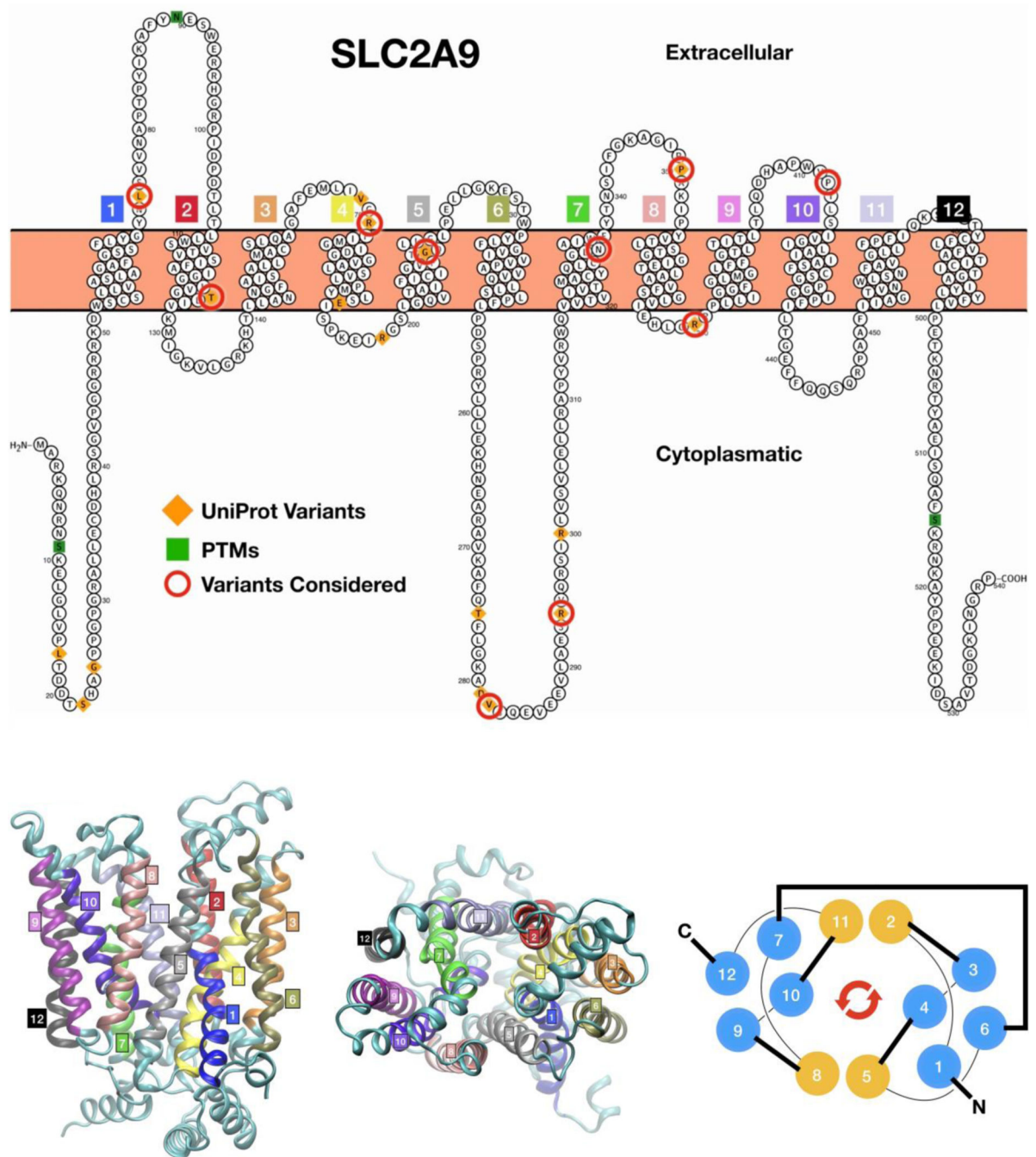
Fig. 1.
Top: *GLUT9* (also known as *SLC2A9b*) membrane organization and mutants; Bottom: model structure overview with pseudosymmetric arrangement and helix numbering convention
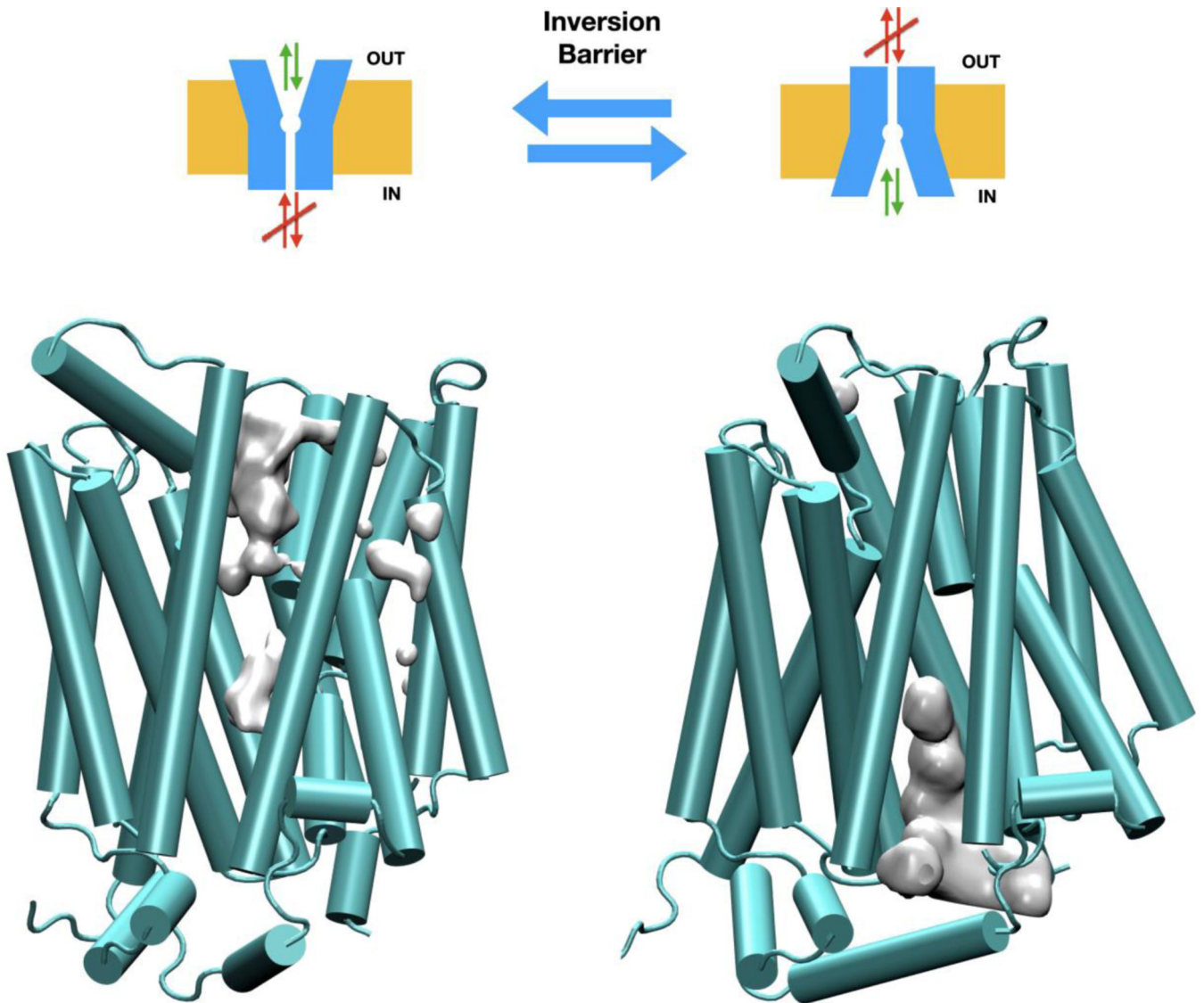
Fig. 2.
Rocket switch (RS)-GLUT transporters in the outward-open or inward-open forms. Notice the change in the vestibular areas indicated by the volumes in grey.
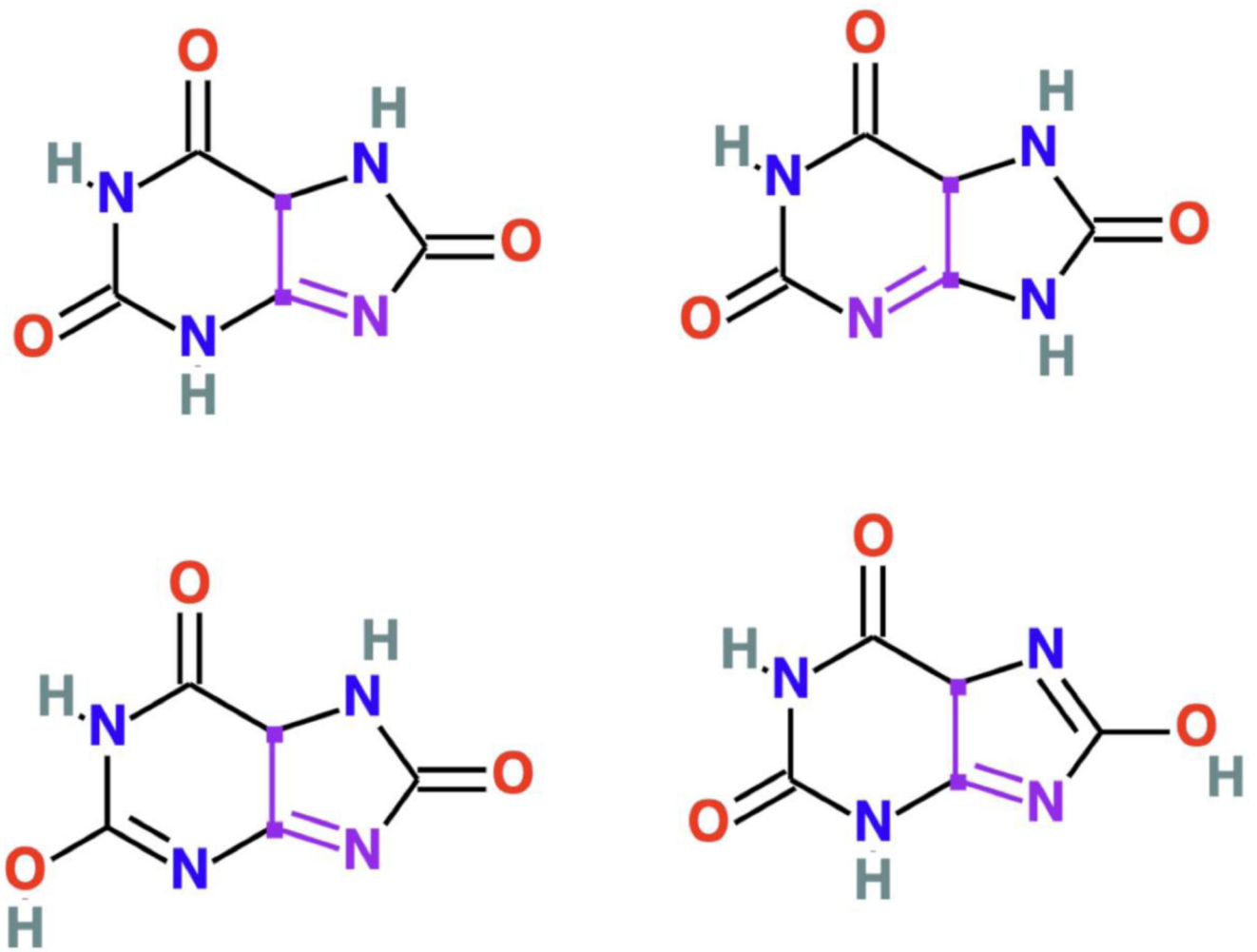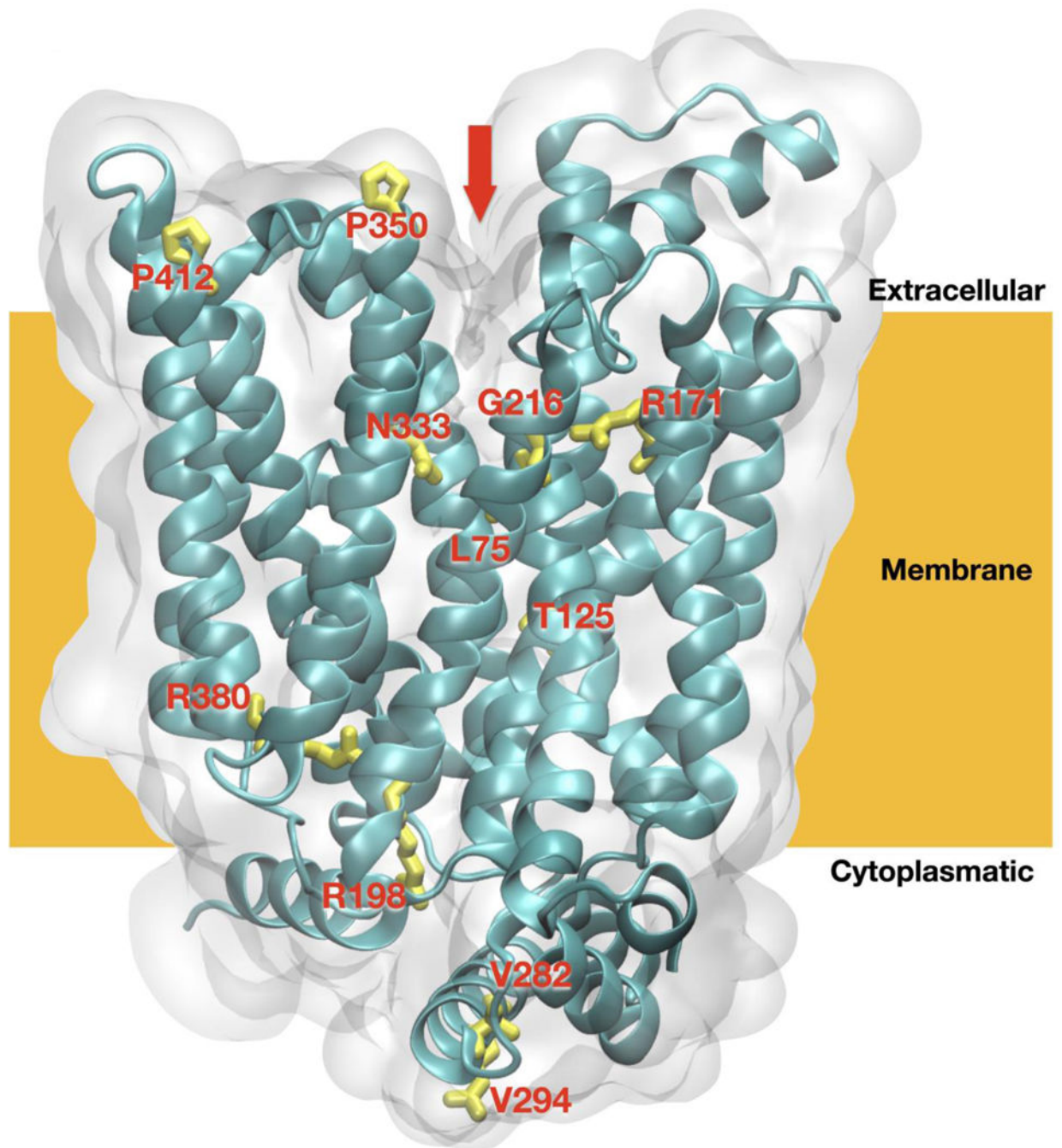
Fig. 3.
Urate tautomers considered.

Fig 4.
GLUT9 model and key residue for hypouricemia; G(Glycine), L(Leucine), N(Asparagine), R(Arginine), T(Threonine), V(Valine),
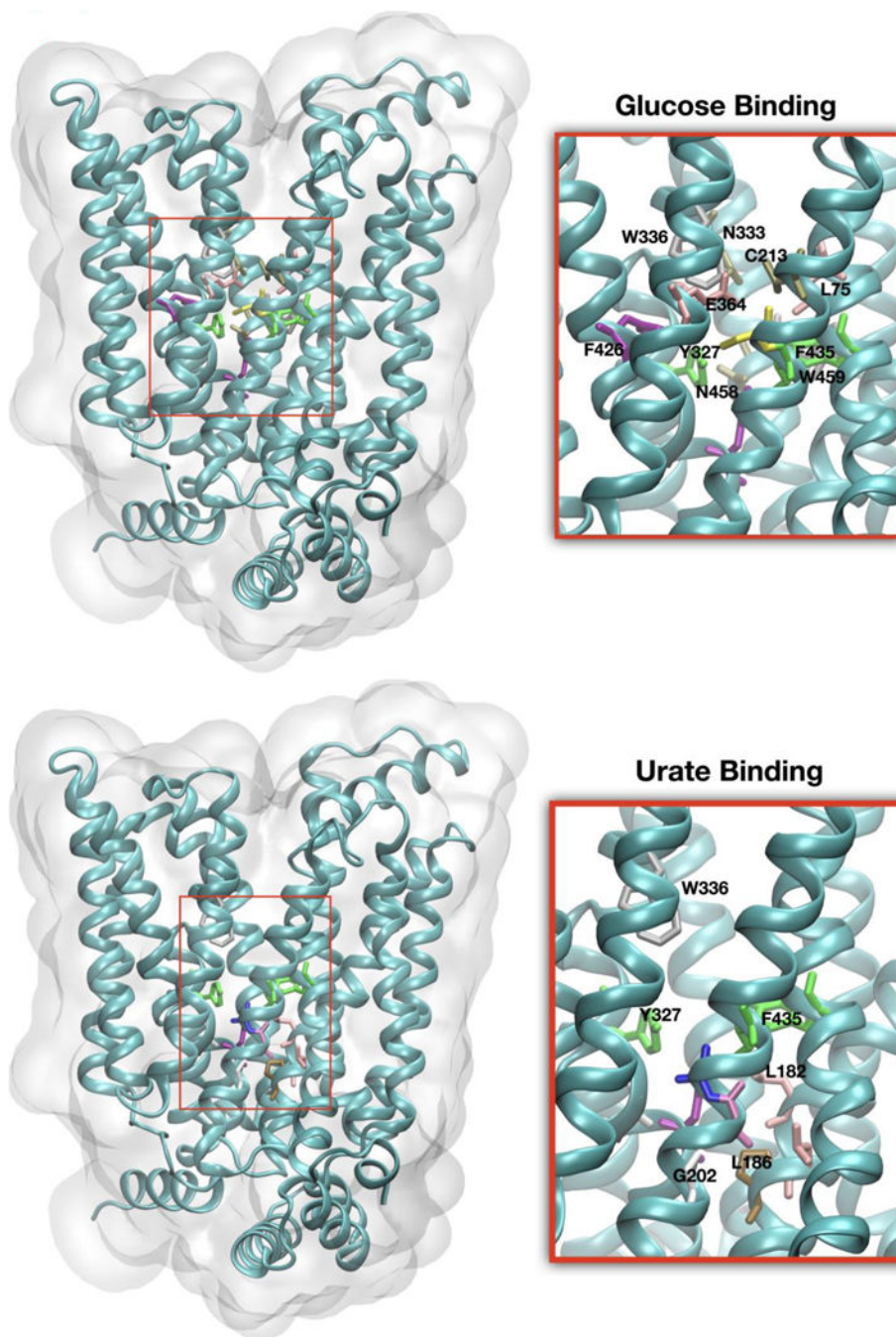
Fig 5.
Top: Glucose binding site for GLUT9, Bottom: Urate binding site for GLUT9; C(Cytosine), E(Glutamate), F(Phenylalanine), G(Glycine), H(Histidine), L(Leucine), N(Asparagine), W(Tryptophan), Y(Tyrosine),

Predicted effect of reported *GLUT9* mutations

Table 1.

Gene symbol	Canonical SPDI (GRCh37)	Amino acid change (NP_064425.2)	Amino acid conservation					dbSNP database (PMID)	gnomAD 2.1.1 MAF	Mutation taster	CLINVAR	CADD_PHRED 1.6	GWAS effect size for gout study	GWAS effect size for urate study
			Rhesus macaque	Mouse	*Xenopus tropicalis*	Lizard	Zebrafish							
GLUT9	4:10022992G>A	p.T21I	T	T	=	X	=	rs748372830 (31131560[47])	4.37 E^{-05}	PM	–	9.426		
	4:10022981C>T	p.G25R	–	G	=	–	=	rs2276961 (19926891[48])	0.51	PM	Benign	3.056	0.12	0.14
	4:10020634C>T	p.G72D	–	-	=	–	=	26500098[49]	6.46 E^{-06}	DC	–	24.9		
	4:10020624A>C	p.L75R	L	L	=	L	=	rs863225072 (19926891[48])	6.37 E^{-05}	DC	Pathogenic	24.9		
	4:9998441G>C	p.T125M	T	T	=	A	A	rs181509591 (21810765[50])	2.39 E^{-05}	DC	Pathogenic	30		
	4:9987317G>A	p.R171C	R	R	R	R	R	rs776127501 (21810765[50])	3.59 E^{-05}	DC	Uncertain Significance	25.0		
	4:9987316C>T	p.R171H	R	R	R	R	R	rs769968441 (27116386[51])	3.98 E^{-05}	DC	Uncertain Significance	26.5		
	4:9982305G>A	p.R198C	R	R	R	=	R	rs121908322 (1902639[52])	3.19 E^{-05}	DC	Likely Benign	29.3		
	4:9982251C>T	p.G216R	G	G	G	G	G	rs561633150 (2252753[53])	5.50 E^{-05}	DC	–	28.6		
	4:9921167C>T	p.V282I	V	V	V	V	V	rs16890979 (1883462[54])	0.245	PM	Benign	9.848	-0.41	-0.33
	4:9922130C>T	p.R294H	R	R	R	R	R	rs3733591 (1972361[55])	0.240	PM	Benign	18.42	-0.07	-0.05
	4:9922013T>C	p.N333S	N	N	N	N	N	rs753482595 (2252753[53])	8.00 E^{-06}	DC	–	22.8		
	4:9909923G>A	p.P350L	P	Q	P	P	=	rs2280205 (19926891[48])	7.96 E^{-06}	PM	Benign	12.69	0.07	0.05
	4:9892311G>A	p.R380W	R	R	–	=	=	rs121908321 (1902639[52])	1.95 E^{-04}	DC	Uncertain Significance	27.9		
	4:9989247G>C	p.P412R	P	P	X	=	=	rs121908323 (1870146[56])	5.75 E^{-06}	DC	Pathogenic	22.3		

Abbreviations: Chr, chromosome; MAF, minor allele frequency from The Genome Aggregation Database (gnomAD v2.1.1); MT, prediction and score from Mutation taster, an algorithm that calculates disease causing potential of sequence alterations; downloaded from ANNOVAR (https://annovar.openbioinformatics.org/en/latest/user-guide/download/DC, disease causing); PM, polymorphism; DC, Disease-Causing; CADD (combined annotation-dependent depletion), prediction and score from ANNOVAR's ljb26_cadd; downloaded from ANNOVAR (https://annovar.openbioinformatics.org/en/latest/user-guide/download/); CLINVAR, database of clinically observed genetic variants; downloaded from http://clinvitae.invitae.com/, and the conservation track from UCSC (https://www.ncbi.nlm.nih.gov/pmc/articles/PMC2099589/); Amino Acid Change, T(Threonine), I(Isoleucine), G(Glycine), R(Arginine), D(Aspartic Acid), L(Leucine), M(Methionine), C(Cytosine), H(Histidine), V(Valine), N(Asparagine), S(Serine), P(Proline), W(Tryptophan), X(Termination)

Table 2.

Urate Transport parameters and the altered transport by mutations.

Urate transport parameters for the wild-type transporter and several mutations discussed in the main text; ΔG_y^x describes the averaged energy values for a given site where X can be O (outwards facing) or I (inward facing) and Y can be i (internal) or e (external) site. ΔG_M^x corresponds to the highest energy point obtain for the path connecting the ΔG_i^x and ΔG_e^x sites. Errors are shown in parenthesis. Note the inversion energy (Inversion) corresponds to the highest energy point obtained for the lowest energy path computed connecting the sites identified as ΔG_i^O and ΔG_i^I and is considered as an upper bound to the actual energy due to the difficulty modeling this inversion process.

	ΔG_e^o	ΔG_M^o	ΔG_i^o	Inversion	ΔG_i^I	ΔG_M^I	ΔG_e^I	SIFT
WT	−6.5(1.8)	−2.6(1.0)	−5.4(1.1)	3.0	−7.8(1.3)	−4.5(1.4)	**−6.1**(1.4)	
L75R	−6.6(1.9)	4.3(1.4)	−1.8(1.2)	6.7	−7.1(0.7)	−5.0(2.1)	−6.5(1.2)	0.02
T125M	−6.5(1.2)	−1.1(1.4)	−3.3(1.1)	5.1	−0.2(0.8)	−2.9(1.3)	−6.2(1.5)	0.00
R171C	−5.8(1.1)	5.5(1.5)	−4.2(1.2)	13.5	−5.9(1.0)	−5.2(1.9)	−5.9(1.2)	0.00
R171H	−6.2(1.2)	−1.7(0.7)	−5.0(0.7)	3.3	−7.0(0.9)	−4.3(1.3)	−6.2(1.3)	0.00
R198C	−6.3(1.0)	−2.0(1.0)	−3.1(1.5)	4.5	−5.6(0.6)	−4.0(1.1)	−6.6(0.9)	0.00
G216R	−6.2(1.8)	4.2(1.3)	−5.0(1.5)	5.1	−5.0(1.0)	−4.0(1.6)	−5.8(1.4)	0.00
V282I	−6.3(1.3)	−2.7(0.8)	−3.1(1.4)	2.8	−6.2(0.7)	−5.0(1.6)	−6.6(0.4)	0.09
R294H	−6.1(1.0)	−2.5(1.2)	−3.7(0.7)	3.2	−6.5(1.2)	−4.1(1.8)	−6.8(0.8)	0.00
N333S	−6.0(1.3)	−0.1(1.0)	−2.0(0.8)	6.0	−3.1(1.3)	−4.5(1.1)	−5.7(1.7)	0.00
P350L	−4.5(1.5)	0.0(1.1)	−4.9(1.3)	2.4	−6.8(0.6)	−4.4(1.9)	−6.0(1.0)	0.06
R380W	−6.5(1.2)	−3.0(1.4)	−3.4(0.9)	17.0	−2.0(1.2)	2.3(1.0)	−6.4(1.3)	0.00
P412R	−4.9(2.0)	1.1(0.9)	−4.8(1.4)	3.3	−6.2(1.2)	−3.4(1.5)	−5.4(0.7)	0.16

Table 3.

Parameters of the *GLUT9* transporter for different substrates. Errors are shown in parenthesis.

	ΔG_e^o	ΔG_M^o	ΔG_i^o	**Inversion**	ΔG_i^I	ΔG_M^I	ΔG_e^I
Urate	**−6.5(0.7)**	−2.6(1.1)	**−5.4(0.3)**	3.0	**−7.8(0.5)**	−4.5(1.7)	**−6.1(1.4)**
Glucose	**−3.4(1.4)**	1.9(1.3)	**−3.5(0.6)**	5.4	**−2.4(1.2)**	−0.4(1.3)	**−4.0(1.2)**
DHA	**−4.2(1.6)**	−1.6(0.7)	**−6.3(1.1)**	2.7	**−3.3(1.3)**	−0.6(0.4)	**−2.9(2.0)**
Chlorine	**−5.0(2.5)**	7.8(1.5)	**−0.5(2.0)**	4.6	**−7.0(1.4)**	2.3(1.8)	**−1.8(1.7)**